ELSEVIER

Journal of Alloys and Compounds 235 (1996) 135–142

Journal of ALLOYS AND COMPOUNDS

Structural and electronic properties of $K_2Ni_3S_4$, a pseudo-two dimensional compound with a honeycomb-like arrangement

Scott H. Elder[a,1], Stéphane Jobic[a], Raymond Brec[a,*], Maria Gelabert[b], Frank J. DiSalvo[b]

[a] *Institut des Matériaux de Nantes, Laboratoire de Chimie des Solides, 44072 Nantes Cedex 03, France*
[b] *Department of Chemistry, Baker Laboratory, Cornell University, Ithaca, New York 14853-1301, USA*

Received 28 April 1995; in final form 12 September 1995

Abstract

Air sensitive single crystals of $K_2Ni_3S_4$ have been synthesized by reaction of 1Ni, $2K_2S$ and 4S in an evacuated silica tube at 750°C for 6 days. The structure was solved in the *Fddd* space group with $a = 5.723(2)$ Å, $b = 10.040(3)$ Å and $c = 26.059(7)$ Å. The refinement led to $R_F = 0.038$ ($R_{wF} = 0.045$) for 23 variables and 392 reflections. The crystal structure can be described along the *c*-axis as the succession of $[Ni_3S_4^{2-}]$ infinite layers separated by two alkali metal cation slabs. In the $[Ni_3S_4^{2-}]$ layers, the nickel atoms are in sulfur square planar coordination. The (NiS_4) square planes are linked together by edge sharing in such a way as to define a honeycomb network. Despite the occurrence of short S···S contacts perpendicular to the slabs, electrical measurements and tight-binding band structure calculations suggest the classical overall charge balance $K_2^{I}Ni_3^{II}S_4^{-II}$.

Keywords: $K_2Ni_3S_4$; Ni^{II}; (NiS_4) square plane; Honeycomb network; Short S···S contacts

1. Introduction

Owing to their high electropositivity and hence the ionic bonding ensuing, alkali metals can be easily intercalated in or deintercalated from low dimensional chalcogenides [1]. With lithium on the one hand and open structure oxides on the other hand, this led to the development of new high energy batteries [2]. Likewise, weakly bonded and easily oxidizable hosts lead readily to deintercalation of alkali-metal-containing ternary phases, yielding in some instances new polymorphs of binary compounds such as VS_2 and CrX_2 (X = S, Se) metastable phases [3–6]. These types of reaction have been a strong incentive for the syntheses of new compounds with alkali metals.

Moreover, through the use of molten alkali-metal polychalcogenides as reagents and solvents, a great variety of low dimensional ternary polychalcogenides containing transition and alkali metals have been recently synthesized by Ibers and co-workers [7] and Kanatzidis [8]. These materials with novel structures show interesting internal redox competitions between anionic and cationic electronic band levels and this urged us to embark on the study of new ternary sulfides.

In addition, as mentioned by Lu and Ibers [9] and Bronger et al. [10], alkali metal content seems to govern the dimensionality of the transition element chalcogenide network. Usually, the dimensionality of binary compounds is lowered by the progressive incorporation of alkali metal (decrease of the transition metal/ alkali metal ratio). For example, ZnS is a 3D-compound, while $Na_2Zn_3S_4$ [9], Na_2ZnS_2 [11,12] and Na_6ZnS_4 [11,12] show respectively a 2D, 1D and 0D character. The probable explanation is that the alkali metals are so electropositive that they do not enter into strong chemical bonding with the chalcogens. As a result, the alkali metal content increase will tend to break up the initial tridimensional iono-covalent bonding, ultimately leading to a lower dimensionality of the system. The alkali metal then appears as a relevant parameter to modify the dimensionality and hence the physical properties of the compounds in which they are introduced.

In view of the interesting character of alkali metal–transition metal sulfides and after the recent synthesis

* Corresponding author.
[1] Current address: Department of Chemistry, University of California, Berkeley, CA 94720, USA.

SSDI 0925-8388(95)02065-9

of a new nickel thiophosphate ($KNiPS_4$) [13] with 1D and 2D structural arrangements, we decided to investigate the previously synthesized $K_2Ni_3S_4$ [14,15]. The single crystal structure of this material had not been solved, presumably because of the lack of high quality single crystals. Crystals of $K_2Ni_3S_4$ had been described as having a gold metallic luster and magnetic susceptibility measurements exhibited weak temperature independent paramagnetism, a behavior not quite expected in the hypothesis of a Ni^{II} in a square sulfur arrangement.

2. Experimental section

2.1. Synthesis and characterization

Single crystals of $K_2Ni_3S_4$ suitable for X-ray analysis were prepared by loading a silica tube with 0.25 g of Ni powder, 1.0 g of K_2S and 0.58 g of S (approximately 4K:1Ni:6S or 1Ni:$2K_2S_3$) in an argon-filled glove box and then sealing the tube under vacuum (10^{-3} Torr). The reaction tube was heated at 20°C h^{-1} to 750°C. held at this temperature for 6 days and then cooled to room temperature at 10°C h^{-1}. The K_2S_3 flux was readily washed away with water, leaving behind hexagonal plates with a gold-metallic luster. It was observed using a light microscope that the edges of all the plates were flared out, revealing the lamellar nature of this material. At this point we presumed that water/oxygen was diffusing between the layers and reacting with this new material causing the large single crystals to be cleaved into thin sheets. To circumvent this problem in subsequent preparations all manipulations of the reaction products were carried out in an argon-filled glove box. Removal of the K_2S_3 flux was accomplished by washing the product with ethylenediamine (dried over freshly activated 3 Å molecular sieves) until no more yellow-orange color remained in solution, indicative that all the K_2S_3 had been removed. The resultant crystals were placed under paraffin oil (dried with freshly activated 3 Å molecular sieves) and were viewed by light microscope under ambient conditions and found not to be cleaved into thin sheets as before; instead they exhibited well defined edges and hexagonal morphology. Single crystals isolated and manipulated in this manner were used in subsequent structural and physical property studies since single phase, polycrystalline powder could not be prepared under a variety of reaction conditions.

Semi-quantitative scanning electron microscopy (SEM) analysis on a variety of the crystals yielded a wide range of stoichiometries. This was likely due to decomposition upon air exposure of the crystals as they were being loaded into the ante-chamber of the microscope. Therefore, the stoichiometry of the material was accurately determined from the single crystal X-ray diffraction data refinement (vide infra).

2.2. Single crystal diffraction

Analysis of rotation and Weissenberg photographs of $K_2Ni_3S_4$ indicated a Laue symmetry m and provided the preliminary cell parameters $a \approx 5.7$ Å, $b \approx 10.2$ Å, $c \approx 13.0$ Å and $\beta \approx 100°$. The systematic extinctions (hkl, $h+k=2n$, and $h0l$, $l=2n$) were consistent with the monoclinic space groups $C2/c$ and Cc. The selected single crystal (less than $0.031 \times 0.075 \times 0.183$ mm^3) was then transferred to a CAD4 Enraf–Nonius single crystal diffractometer. The cell parameters were refined to the values $a = 5.708(2)$ Å, $b = 10.027(2)$ Å, $c = 13.308(1)$ Å, and $\beta = 102.38(1)°$. A search for a higher symmetry ended with the orthorhombic cell $a = 5.708(2)$ Å, $b = 10.027(2)$ Å and $c = 25.995(6)$ Å ($a_{ortho} = -a_{mono}$, $b_{ortho} = b_{mono}$, $c_{ortho} = -a_{mono} - 2c_{mono}$) with an F centered Bravais lattice. The final cell were determined from a least squares analysis of the setting angles of 30 centered reflections in the range $15° < 2\theta Mo(L_{III}) < 30°$. The detailed recording conditions are reported in Table 1. To allow for semi-empirical absorption corrections, psi measurements of the intensities of two $\chi \approx +90°$ reflections were undertaken. The usual corrections (i.e. absorption and Lorentz and polarization) were applied. Diffracted intensities were averaged in agreement with the Laue symmetry mmm. From the 4228 collected reflections and after averaging in the $Fmmm$ symmetry, 392 independent reflections with $I > 3\sigma(I)$ were finally left for the refinements with agreement factors on the intensity averaging of 5.7%. Note the need to have a rather large omega scan angle ($1.9° + 0.35°\mathrm{tg}\theta$) to record the diffraction peaks related to the average quality of the crystal. Also, because of its air sensitivity, the crystal was covered with mineral oil to avoid oxidation and/or water reaction and loaded into a thin (0.2 mm diameter) Lindeman capillary.

2.3. Powder diffraction

The accurate cell parameters of $K_2Ni_3S_4$ were then determined by least squares refinement from data collected on a CPS 120 INEL X-ray powder diffractometer using a monochromatized radiation Cu K-L_{III} ($\lambda = 1.540598$ Å) and equipped with a position-sensitive curve detector calibrated with $Na_2Ca_3Al_{12}F_{14}$ as a standard (cubic compound with $a = 10.2501(1)$ Å). In view of the air-sensitive character of the compound, the powder was sealed in a 0.2 mm diameter glass capillary. The refinement of the diagram in the 10–100° 2θ range yielded $a = 5.723(2)$ Å, $b = 10.040(3)$ Å, $c = 26.059(7)$ Å with a 2θ average deviation of 10/1000. Table 2 shows the observed and calculated d

Table 1
Analytical and crystallographic data parameters of the X-ray collection refinement

Physical, crystallographic and analytical data
Formula: $K_2Ni_3S_4$
Molecular weight: 382.54 g mol^{-1}
Color: gold
Compound highly air-sensitive
Crystal symmetry: orthorhombic
Space group: *Fddd* (No. 70)
Cell parameters at room temperature refined from X-ray powder diagram:
$a = 5.723(2)$ Å, $b = 10.040(3)$ Å, $c = 26.059(7)$ Å
Volume: 1497(1) $Å^3$
$Z = 8$
Density: $\rho = 3.39$ g cm^{-3}
Crystal size: $<0.031 \times 0.075 \times 0.183$ mm^3
Linear absorption: $\mu = 96.5$ cm^{-1}

Data collection
Diffractometer: Enraf–Nonius CAD-4F
Temperature: 293 K
Radiation: Mo K – L_{III}
Monochromator: oriented graphite (002)
Scan mode: ω/θ
Scan angle: $1.9° + 0.35°\mathrm{tg}\theta$
Recording angle: 1.5–35°
Standard reflections: (−2 2 0), (−2 6 0), (−2 −2 −8)
Period of intensity control: 3600 s
Period of orientation control: 200

Refinement condition
Space recorded: $-9 \leq h \leq 9$; $-4 \leq k \leq 16$; $-42 \leq l \leq 42$
Recorded reflections: 4228
Independent reflections ($I > 3\sigma(I)$): 392
$R_1 = \Sigma\,|I - I_{ave}|/\Sigma\, I = 5.7\%$
Refined parameters: 23
Reliability factors:
$R_F = \Sigma\,\|F_o| - |F_c\|/\Sigma\,|F_o|$, $R_{wF} = (\Sigma\, w(|F_o| - |F_c|)^2/\Sigma\, w|F_o|^2)^{1/2}$
Weighting scheme: $w^{-1} = (\sigma^2(F_o) + 0.06F_o^2)^2$

Refinement results
$R_F = 3.8\%$ $R_{wF} = 4.5\%$
Goodness of fit: $S = 1.75$
Difference Fourier maximum and minimum peak intensity: 1.41/−1.28 e^- $Å^{-3}$

spacings along with the observed and calculated intensities [16]. The occurrence of rather few peaks is attributed not only to the Bravais lattice of the phase, but also to the large amount of NiS present in the bulk material, making difficult the observation of the weakest $K_2Ni_3S_4$ lines. Also, some preferred orientation may have weakened some lines, although the capillary geometry is less sensitive to that phenomena than the plate geometry.

2.4. Structure determination

The structure was solved from the three-dimensional Patterson map and successive Fourier and difference Fourier map analyses using the XTAL3.2 structure determination package [17]. Conventional atomic and anomalous scattering factors were taken from the International Tables for X-Ray Crystallography [18,19].

A data analysis confirmed the *mmm* Laue symmetry with the limiting reflection conditions consistent with the *Fddd* group. The structure was then refined by analogy with $K_2Pd_3S_4$ [20] with Ni atoms in crystallographic sites 8a and 16g, S atoms in site 32h and K in site 16g. The final cycle of the isotropic refinement on F on ten variables and 392 independent reflections converged to an R_F value of 0.053. Anisotropic atomic displacement parameters refinement (23 variables) yielded $R_F = 0.038$ and $R_{wF} = 0.045$ with reliable atomic displacement parameter (ADP). The final difference electron density showed no feature higher than 1.41 e^- $Å^{-3}$ and no lower than −1.28 e^- $Å^{-3}$. The secondary extinction parameter was not taken into account. Final values of the atomic parameters and anisotropic ADPs are given in Tables 3 and 4.

Table 2
Observed and calculated d spacings (Å) for $K_2Ni_3S_4$ ($a = 5.723(2)$ Å, $b = 10.040(3)$ Å, $c = 26.059(7)$ Å, $V = 1497(1)$ $Å^3$) and observed and calculated intensities determined from the Lazy Pulverix program

hkl	d_{obs}	d_{calc}	I_{obs}	I_{calc}
004	6.52	6.51	100	100
022	4.683	4.684	18	17
113	4.313	4.315	8	25
115	3.596	3.598	8	23
026	3.287	3.285	11	16
131	2.8724	2.8714	17	21
220	2.4890	2.4860	22	23
206	2.3893	2.3895	18	25
044	2.3413	2.3422	7	8
224	2.3223	2.3226	14	17
137	2.2826	2.2824	14	27
0012	2.1714	2.1716	7	8

Average 2θ angle deviation: 10/1000°.

Table 3
Atomic coordinates and equivalent isotropic ADPs

	x	y	z	B_{eq} ($Å^2$)
Ni(1)	1/8	1/8	1/8	0.92(3)
Ni(2)	3/8	3/8	0.12443(5)	0.85(2)
K	5/8	1/8	0.04451(9)	1.73(5)
S	0.1292(4)	−0.0413(2)	0.06876(7)	1.08(9)

Isotropic equivalent thermal factor defined as $B_{eq} = 4/3\ \Sigma_i\ \Sigma_j\ \beta_{ij} a_i a_j$.

3. Structure description and discussion

Fig. 1(a) shows a projection of the structure in the (010) plane and the labeling scheme. $K_2Ni_3S_4$ is built upon the stacking along the c-axis of cationic–anionic layers along the–[K–S–Ni–S–K]–sequence. Thus, the crystal structure can be described as the succession

Table 4
Anisotropic ADPs

	U_{11}	U_{22}	U_{33}	U_{12}	U_{13}	U_{23}
Ni(1)	0.0127(7)	0.0082(8)	0.0143(7)	0	0	0
Ni(2)	0.0111(4)	0.0076(5)	0.0139(4)	−0.0010(5)	0	0
K	0.023(1)	0.020(1)	0.022(1)	−0.002(2)	0	0
S	0.0160(7)	0.0107(8)	0.0143(7)	0.000(1)	0.0002(8)	−0.0006(6)

The expression of the general temperature factor is

$$\exp[-2\pi^2(U_{11}h^2a^{*2} + U_{22}k^2b^{*2} + U_{33}l^2c^{*2} + 2U_{12}hka^*b^* + 2U_{13}hla^*c^* + 2U_{23}klb^*c^*)].$$

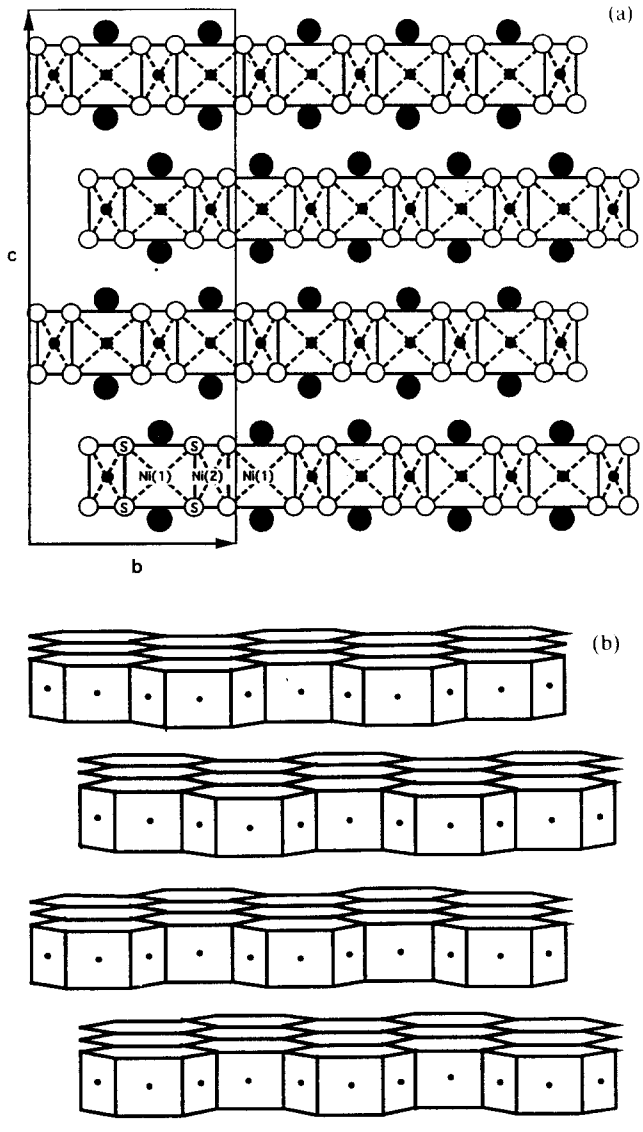

Fig. 1. (a) View down the a-axis of $K_2Ni_3S_4$ showing the labeling scheme and unit cell outline. The small solid circles are Ni atoms, the open circles are S atoms and the large striped circles are K atoms. (b) Perspective view of $^2_\infty[Ni_3S_4^{2-}]$ sandwich stacking.

along the c-axis of $[Ni_3S_4^{2-}]$ sandwiches, seen in perspective in Fig. 1(b), separated by two alkali metal cation $[2K^+]$ sheets giving the compound a bidimensional character. A view down the c-axis given in Fig.

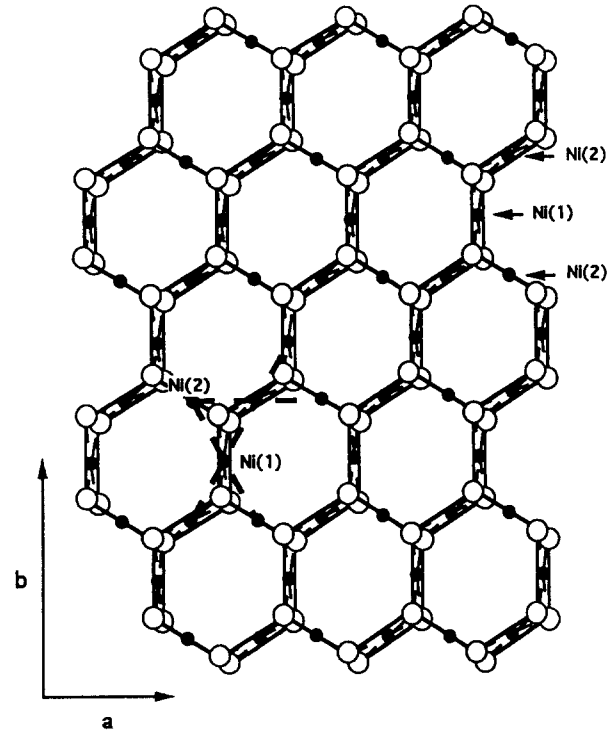

Fig. 2. Perspective view down the c-axis of a $^2_\infty[Ni_3S_4^{2-}]$ sandwich showing the honeycomb-like arrangement. The small solid circles are Ni atoms and the open circles are S atoms. The broken lines represent the Ni rectangular coordination of nickel atoms.

2 shows the labeling scheme and the nickel atom arrangement in a $^2_\infty[Ni_3S_4^{2-}]$ sandwich. Such a sandwich consists of nickel in a slightly distorted sulfur square planar coordination, the sulfur square groups being perpendicular to the (001) plane. The cis-angles S–Ni–S range from 82.57(7) to 97.44(7)° for Ni(1) and from 82.90(8) to 98.39(9)° for Ni(2). The Ni–S distances are very close to one another, with a mean value of 2.221(2) Å and 2.214(2) Å respectively for Ni(1) and Ni(2). This compares well with the previously studied compounds also containing square planar (NiS_4) groups ($Cs_2Ni_3S_4$ [21], $Ta_2Ni_3S_8$ [22], $Pt_5Pd_2NiS_8$ [23], $KNiPS_4$ [13]) and the nickel cations can be considered as Ni^{II} species with a low spin configuration d^8 as they often are in such compounds. The above Ni–S distances give an effective ionic radius for Ni^{II} of about 0.38 Å ($R_{S^{2-}} = 1.84$ Å), a rather small value compared with that of 0.49 Å given by Shannon [24].

The (NiS_4) square planes are linked together by edge sharing in such a way as to define a honeycomb network (Fig. 2). In addition, each Ni atom is rectangularly coordinated in a plane parallel to (001) by four metals (broken lines in Fig. 2). The Ni(2)–Ni(1)–Ni(2) angles equal 59.37(2) and 120.63(2)°, while the Ni(2)–Ni(2)–Ni(2) angles equal 60.31(1) and 119.68(1)°. The Ni–Ni distances that range from 2.862(1) to 2.8892(7) Å, i.e. about 8% higher than the Ni···Ni contacts in nickel metal, could be attributed to bonding interactions. Such a possibility is to be discussed below (see band structure section below).

Between the $^2_\infty[Ni_3S_4^{2-}]$ layers, the K^+ cations are in an eight sulfur coordination polyhedra corresponding to six sulfur rings from one (Ni_3S_4) slab and two sulfur atoms from the neighboring (Ni_3S_4) slab. The (KS_8) polyhedron is represented in Fig. 3. The potassium coordination can also be viewed as a bicapped trigonal prism, the bicapping taking place through the prism's triangles. The mean K–S distance equals 3.383(3) Å, in good agreement with the sum of the van der Waals radius of K^+ and S^{2-} ($d = 3.35$ Å [25]). The potassium atom shares six bonds with S atoms of a $^2_\infty[Ni_3S_4^{2-}]$ block (3.352(3) (×2), 3.393(3) (×2), and 3.410(2) (×2) Å) and two bonds with another block (3.376(3) (×2) Å). Note that one observes a simple stacking of two $^2_\infty[Ni_3S_4^{2-}]$ sandwiches in $Cs_2Ni_3S_4$ [21] (Fig. 4(a)), while in $K_2Ni_3S_4$ the sequence is that of four layers stacked as shown in Fig. 4(b). Other types of stacking can be imagined, like that found for the $^2_\infty[Pt_3S_4^{2-}]$ layers in $Cs_2Pt_3S_4$ [25] (Fig. 4(c)).

Examining the values of the S–S distances in Table 5, short S···S contacts within planar (NiS_4) entities are found. Perpendicular to the (001) plane, some chalcogen–chalcogen distances are as short as 2.931(3) Å and compared well with the S···S distances for shared sides found in $Cs_2Ni_3S_4$ (2.897 and 2.879 Å) [21], $K_2Pd_3S_4$ (3.06 Å) [20], $Rb_2Pd_3S_4$ (3.09 Å) [20],

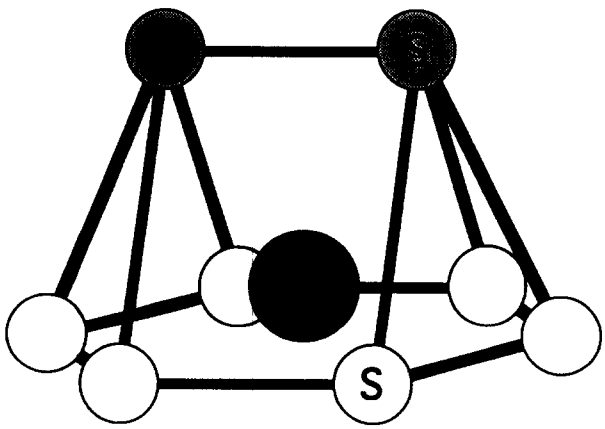

Fig. 3. Perspective view of a (KS_8) polyhedron. The six sulfur atoms of the hexagonal ring (open circles) belong to a $^2_\infty[Ni_3S_4^{2-}]$ block, while the two others are members of a second block (shaded circles).

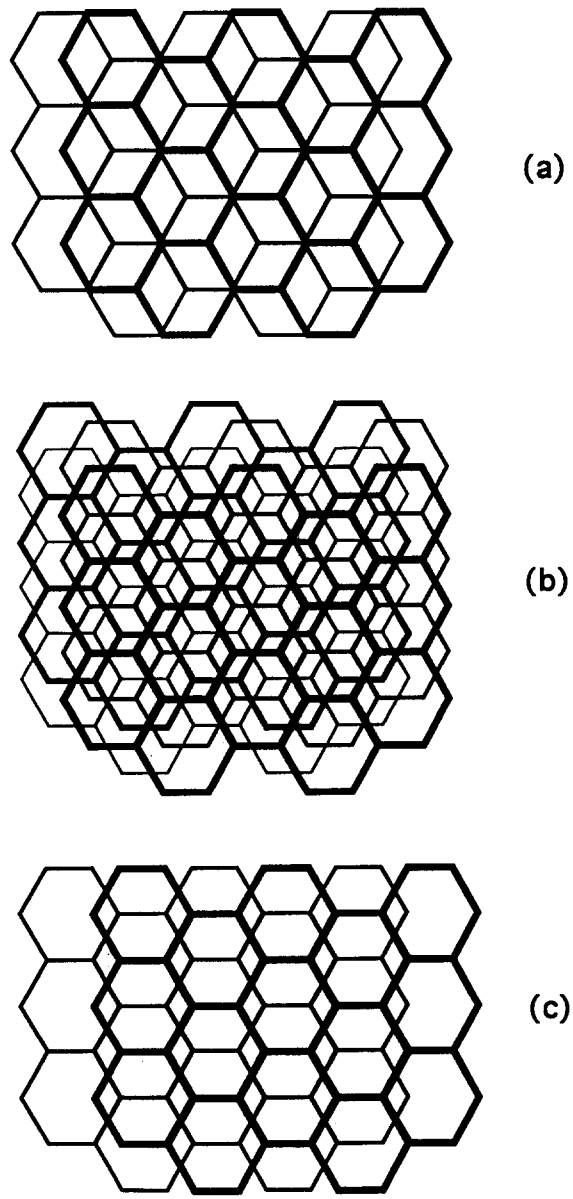

Fig. 4. Stacking of $^2_\infty[M_3S_4^{2-}]$ sandwiches (M = Ni, Pd) in $Cs_2Ni_3S_4$ (a), $K_2Ni_3S_4$ (b), and $Cs_2Pt_3S_4$ (c). The hexagons represent a 2D-$[M_3S_4]$ sandwich.

$Cs_2Pd_3S_4$ (3.00 Å) [26] and $Cs_2Pt_3S_4$ (3.155 Å) [25]. Such a value is intermediate between S–S pairs contacts of about 2.05 Å as observed in semiconducting phases such as PV_2S_{10} [27], $P_2Nb_4S_{21}$ [28], PNb_2S_{10} [29] and $Ta_4P_4S_{29}$ [30] and pyrite compounds [31] for instance and $S^{2-}\cdots S^{2-}$ contact distances of about 3.46 Å as calculated in lamellar TiS_2. Such short S–S distances could be the signature of bonding interactions between chalcogens in relation with a depletion of the most antibonding levels of the sulfur anionic band. Such a hypothesis will be explored in the next section from an electronic band structure point of view. Note, however, that short sulfur–sulfur contact distances of $d_{S-S} = 2.995$ Å and 2.972 Å were found in

Table 5
Mean interatomic distances (Å) and angles (deg) with their estimated deviations

Ni(1) environment			
Ni(1)–S	2.221(2) (×4)	S–Ni(1)–S	97.44(7) (×2)
S–S	2.931(3) (×2)	S–Ni(1)–S	82.57(7) (×2)
S–S	3.339(3) (×2)	S–Ni(1)–S	178.76(9) (×2)
Ni(1)–Ni(2)	2.8892(7) (×4)	Ni(2)–Ni(1)–Ni(2)	59.37(2) (×2)
		Ni(2)–Ni(1)–Ni(2)	120.63(2) (×2)
		Ni(2)–Ni(1)–Ni(2)	179.42(5) (×2)
Ni(2) environment			
Ni(2)–S	2.208(2) (×2)	S–Ni(1)–S	95.82(9) (×1)
Ni(2)–S	2.220(2) (×2)	S–Ni(1)–S	98.39(9) (×1)
S–S	2.931(3) (×2)	S–Ni(1)–S	82.90(8) (×2)
S–S	3.361(4) (×1)	S–Ni(1)–S	178.57(9) (×2)
S–S	3.278(4) (×1)		
Ni(2)–Ni(1)	2.8892(7) (×2)	Ni(1)–Ni(2)–Ni(2)	60.31(1) (×2)
Ni(2)–Ni(2)	2.862(1) (×2)	Ni(2)–Ni(2)–Ni(2)	119.68(1) (×2)
		Ni(1)–Ni(2)–Ni(1)	179.42(3) (×1)
		Ni(2)–Ni(2)–Ni(2)	178.82(7) (×1)
K environment			
K–S	3.352(3) (×2)	S–K–S	59.21(6) (×2)
K–S	3.376(3) (×2)	S–K–S	57.98(6) (×2)
K–S	3.393(3) (×2)	S–K–S	59.34(5) (×2)
K–S	3.410(2) (×2)	S–K–S	85.43(5) (×2)
S–S	3.361(4) (×2)	S–K–S	71.70(5) (×2)
S–S	3.278(4) (×2)	S–K–S	86.34(6) (×2)
S–S	3.339(3) (×2)	S–K–S	58.07(7) (×1)
S–S	3.965(3) (×2)[a]		
S–S	4.6033(3) (×4)[a]		
S–S	3.278(4) (×1)		

[a] Interslab distances.

PV_2S_{10} [27] and $V(S_2C_2(C_6H_5)_2)_3$ [32] respectively, and were ascribed to steric effects. Such a situation was also met in IrS_2 with a slightly higher S–S distance of 3.003(9) Å [33].

4. Magnetic susceptibility

Temperature dependent magnetic susceptibility measurements were performed on a Quantum Design SQUID magnetometer. 12.1 mg of single crystals of $K_2Ni_3S_4$ were picked out and loaded into a Kel-F bucket fitted with an air-tight, screw-top cap in an argon-filled glove box. Data were collected from 4.2 to 290 K at 5 and 40 kG. The sample exhibits a very weak field dependence, indicating the presence of small amount of ferromagnetic impurity. The data were corrected by subtracting the sample container signal and the core diamagnetism (K^+: -13×10^{-6}, Ni^{2+}: -12×10^{-6}, S^{2-}: -38×10^{-6} emu mol^{-1}) resulting in essentially independent, weak paramagnetism (with a Curie tail at low T) with an average susceptibility (in the 50 K to room temperature range) of about $8.6(5)\times10^{-5}$ emu mol^{-1} for $H=40$ kG. However, much caution had to be exercised interpreting the susceptibility owing to the weak signal and the somewhat scattered data. In effect, considering the deviation range and the incertitude on Pascal constants, not to mention again some preferred orientation, the phase could very well be diamagnetic. Note that electronic calculations by the extended Hückel method evidences a semiconductor or insulator behavior (vide infra).

5. Resistivity measurements

Owing to the inconclusive nature of the magnetic susceptibility data just described, electrical resistivity measurements were made to better understand the electronic character of $K_2Ni_3S_4$. The temperature dependence of the four-probe resistivity was measured on a small, flat crystal fragment of dimension $0.7\times1.0\times0.06$ mm^3 in a nitrogen gas filled glove-bag to prevent air exposure. Contacts were made on the edge of the sample with silver paint, and van der Pauw measurements were made by lock-in detection [34]. The room temperature resistivity was 1.9(3) Ω cm.

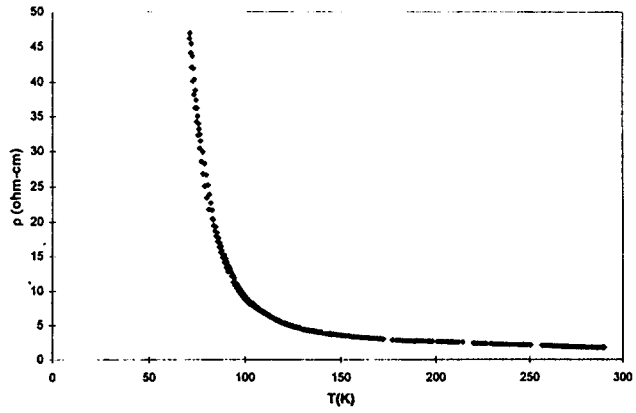

Fig. 5. Electrical behavior of $K_2Ni_3S_4$ from room temperature down to liquid nitrogen.

The contact resistances were about 150 Ω, and were ohmic over a 1 V range. Resistivity as a function of temperature down to liquid nitrogen is shown in Fig. 5.

The resistivity vs. temperature data for $K_2Ni_3S_4$ clearly indicates semiconducting behavior with an energy of activation E_a of 0.03 eV ($\rho = \rho_0 \exp(-E_a/2kT)$). The measured E_a is small compared with the theoretically calculated value of 1.8 eV (vide infra), which strongly suggests that $K_2Ni_3S_4$ is an extrinsic semiconductor owing to the presence of donor and/or acceptor impurities within the band gap. These resistivity data suggest that the Ni in $K_2Ni_3S_4$ are Ni^{2+} with a low-spin d^8 electronic configuration surrounded by a square plane of S, where the shortened S–S contacts do not give rise to any appreciable S–S interaction and can be described as S^{2-}. However, if the low activation energy and high room temperature conductivity were intrinsic properties, this could be attributed to bonding S···S contacts and to the occurrence of Ni^{II} and Ni^{I} for instance. This nickel mixed valence state could explain the transport properties for $K_2Ni_3S_4$.

6. Electronic structure

Tight-binding band structure calculations were carried out [35] using an extended Hückel-type Hamiltonian [36]. A modified Wolfsberg–Helmholtz formula was used to calculate the non-diagonal $H_{\mu\nu}$ values [37]. The ionization potentials (electron-volts) and exponents used were: −20.0 and 1.817 for S 3s, −13.3 and 1.817 for S 3p, −9.70 and 2.10 for Ni 4s, −5.15 and 2.10 for Ni 4s, −5.15 and 2.10 for Ni 4p. Double-ξ-type orbitals were used for Ni 3d. The ionisation potential exponents and contractions coefficients were: −13.49, 5.75, 2.30, 0.57979 and 0.57819 respectively. Band structure calculations were performed using a 150 k-point mesh for the irreducible 2D orthorhombic cell. Density of state (DOS) curves were smoothed with a half-width of 0.05 eV. Electronic calculations for a $^2_\infty[Ni_3S_4^{2-}]$ layer were carried out to aid in the understanding of the nature of the short Ni···Ni and S···S contacts.

The total DOS diagram is shown on Fig. 6. The dashed vertical line indicates the highest occupied energy level. The calculations indicate that the compound should be semiconductor with a 1.8 eV energy gap. The occurrence of such a gap unambiguously asserts a low spin d^8 configuration of Ni. The projected DOS shows that the lowest empty band contribution comes from the Ni d orbital usually called $d_{x^2-y^2}$ for a square planar coordination and sp sulfur orbitals. Such an observation suggests a high hybridization of nickel and sulfur orbitals. Notice that the integrated overlap population at the Fermi level for the three types of Ni–S bond (2.221(2) Å, 2.208(2) Å, 2.220(2) Å) fall in the expected range (0.406, 0.409, 0.407 e^-/bond) for low spin configuration of nickel(II) and compares well with the value calculated in $KNiPS_4$ [13]. Otherwise, the integrated calculated overlap populations (IOPOP) at the Fermi level for the Ni···Ni contacts are all negative (−0.015 e^-/bond for Ni(1)–Ni(2) and Ni(2)–Ni(2) contacts) indicating a nonbonding cationic interaction. Such a result is not surprising and has to be understood as a non-overlap between the occupied d orbitals of Ni. In addition, the IOPOP for the 2.931(3) Å S···S contacts (S···S distances perpendicular to the $^2_\infty[Ni_3S_4^{2-}]$ sandwiches) turned out to be positive (+0.036 e^-/bond). An electronic transfer from the sp anionic band to the '$d_{x^2-y^2}$' cation orbital could take place, while maintaining the semiconducting property of the phase if no metallic band were formed upon transfer. However, calculations done on

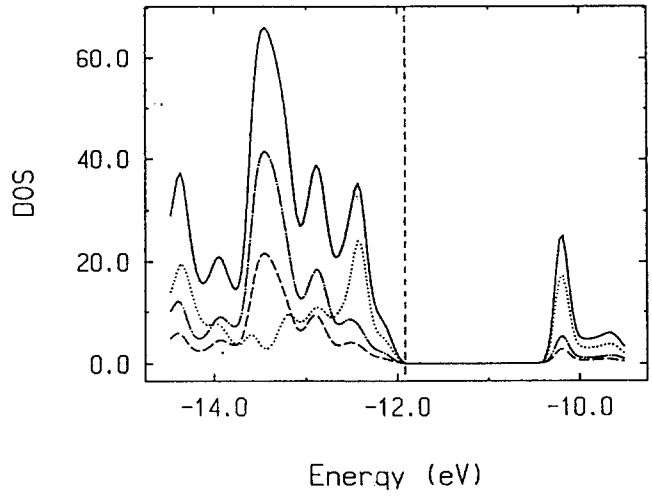

Fig. 6. Total and projected density of states curves. The solid line refers to the total density of states, while the two dashed lines and the dotted one refer to the projected DOS for Ni(1), Ni(2) and S respectively. The last occupied line is represented by the chain line.

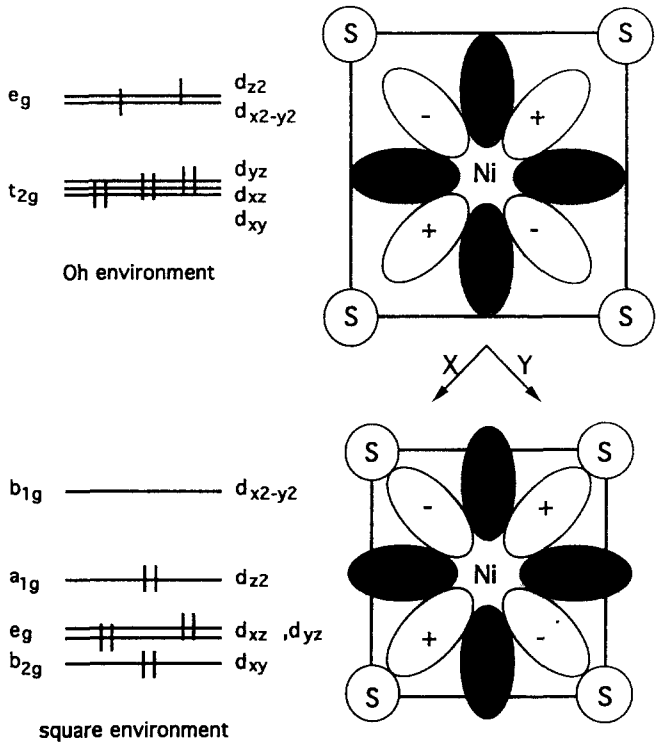

Fig. 7. Influence of the filling of the $d_{x^2-y^2}$ orbital on the metal–chalcogen distance. Much shorter distances are observed in a nickel square environment with short S···S contacts in non-bonding interaction.

$(NiS_4)^{6-}$, $(Ni_2S_6)^{8-}$ and $(Ni_3S_8)^{10-}$ clusters suggest that the positive IOPOP may be an artifact owing to quantum normalization and thus without chemical meaning. Pending further band structure types of calculation, the charge balance $K_2^{I}Ni_3^{II}S_4^{-II}$ with paired electrons and an empty conduction band seems to be retained for the time being. The short Ni···S and S···S contacts would originate mostly from the low spin d^8 configuration of Ni in its square environment (full occupied b_{2g}, e_g, a_{1g} levels and empty b_{1g} level). The empty b_{1g} level (the so-called $d_{x^2-y^2}$ orbital) suggests the possibility for sulfur to get closer to the cation; (this is not the case for a Ni^{II} in an octahedral environment where the e_g orbitals are equally occupied). Short Ni···S distances in $(NiS_4)^{6-}$ thus must originate from a modification of the electrostatic repulsion between S^{2-} and Ni^{2+} compared with a $(NiS_6)^{10-}$ octahedron giving rise to shorter S···S contacts. Such a steric phenomenon is illustrated on Fig. 7.

References

[1] W. Müller-Warmuth and R. Schöllhorn (eds.), *Progress in Intercalation Research*, Kluwer Academic Publishers, 1994.
[2] J. Broahead and M. Farley (eds.), Proc. 7th Int. Meet. on Lithium Batteries, Boston, USA, May 15–20, 1994, *J. Power Sources*, *54* (1995) 1.
[3] D.W. Murphy, J.N. Carides, F.J. DiSalvo, C. Cros and J.V. Waszczak, *Mater. Res. Bull.*, *12* (1977) 825.
[4] D.W. Murphy and J.N. Carides, *J. Electrochem. Soc.*, *126* (1979) 749.
[5] V. Manev, R.V. Moshtev, A. Nassalevska and G. Pistoia, *Solid State Ionics*, *13* (1984) 181.
[6] C.F. VanBruggen, R.J. Haange, G.A. Wiegers and D.K.G. DeBoer, *Physica B*, *99* (1980) 166.
[7] J.A. Cody, M.F. Mansuetto, S. Chien and J.A. Ibers, *Mater. Sci. Forum*, *152–153* (1994) 35.
[8] M.G. Kanatzidis, *Chem. Mater.*, *2* (1990) 353.
[9] Y.-J. Lu and J.A. Ibers, *Comments Inorg. Chem.*, *14* (1993) 229.
[10] W. Bronger and P. Müller, *J. Less-Comm. Met.*, *100* (1984) 241.
[11] K.O. Klepp and W. Bronger, *Z. Kristallogr.*, *162* (1983) 134.
[12] K.O. Klepp and W. Bronger, *Rev. Chim. Minér.*, *20* (1983) 682.
[13] S.H. Elder, A. Van der Lee and R. Brec, *J. Solid State Chem.*, *116* (1995) 107.
[14] W. Bronger, J. Eyck, W. Rüdorff and A. Stössel, *Z. Anorg. Allg. Chem.*, *375* (1970) 1.
[15] W. Bronger, R. Rennau and D. Schmitz, *Z. Anorg. Allg. Chem.*, *597* (1991) 27.
[16] R. Yvon, W. Jeitschko and E. Parthé, *J. Appl. Crystallogr.*, *10* (1977) 73.
[17] S.R. Hall, H.D. Flack and J.M. Stewart (eds.), XTAL3.2 Reference Manual, 1992, Universities of Western Australia, Geneva and Maryland.
[18] D.T. Cromer and J.T. Waber, in J.A. Ibers and W.C. Hamilton (eds.), International Tables for X-Ray Crystallography, Vol. IV, Kynoch, Birmingham, UK, 1974, pp. 72–98.
[19] D.T. Cromer, in J.A. Ibers and W.C. Hamilton (eds.), International Tables for X-Ray Crystallography, Vol. IV, Kynoch, Birmingham, UK, 1974, pp. 149–150.
[20] J. Huster and W. Bronger, *J. Solid State Chem.*, *11* (1974) 254.
[21] W. Bronger, R. Rennau and D. Schmitz, *Z. Kristallogr.*, *183* (1988) 201.
[22] P.J. Squattrito, S.A. Sunshine and J.A. Ibers, *J. Solid State Chem.*, *64* (1986) 261.
[23] J.D. Childs and S.R. Hall, *Acta Crystallogr. Sect. B*, *29* (1973) 1446.
[24] R.D. Shannon, *Acta Cryst. Sect A*, *32* (1976) 751.
[25] O. Günther and W. Bronger, *J. Less-Comm. Met.*, *31* (1973) 255.
[26] W. Bronger and J. Huster, *J. Less-Comm. Met.*, *23* (1971) 67.
[27] R. Brec, G. Ouvrard, M. Evain, P. Grenouilleau and R. Rouxel, *J. Solid State Chem.*, *47* (1983) 174.
[28] R. Brec, M. Evain, P. Grenouilleau and R. Rouxel, *Rev. Chim. Minér.*, *20* (1983) 283.
[29] R. Brec, P. Grenouilleau, M. Evain and J. Rouxel, *Rev. Chim. Minér.*, *20* (1983) 295.
[30] M. Evain, M. Queignec, R. Brec and J. Rouxel, *J. Solid State Chem.*, *56* (1985) 148.
[31] G. Brostingen and A. Kjekshus, *Acta Chem. Scand.*, *23* (1969) 2186.
[32] M. Evain, R. Brec and M.-H. Whangbo, *J. Solid State Chem.*, *71* (1987) 244.
[33] S. Jobic, P. Deniard, R. Brec, J. Rouxel, M.G.B. Drew and W.I.F. David, *J. Solid State Chem.*, *89* (1990) 315.
[34] L.J. Van der Pauw, *Philips Res. Rep.*, *13* (1958) 1.
[35] M.-H. Whangbo and R. Hoffmann, *J. Am. Chem. Soc.*, *100* (1978) 6093.
[36] R. Hoffmann, *J. Chem. Phys.*, *39* (1963) 1397.
[37] J.H. Ammeter, H.-B. Bürgi, J. Thibeault and R. Hoffmann, *J. Am. Chem. Soc.*, *100* (1978) 3686.